Dynamic Tire Friction Models for Vehicle Traction/Braking Control

Carlos Canudas de Wit, Panagiotis Tsiotras, Efstathios Velenis, Michel Basset, Gérard Gissinger

Dynamic Tire Friction Models for Vehicle Traction/Braking Control

Carlos Canudas-de-Wit*
Laboratoire d'Automatique de Grenoble, UMR CNRS 5528
ENSIEG-INPG, B.P. 46, 38 402 ST. Martin d'Hères, FRANCE

Panagiotis Tsiotras, Efstathios Velenis†
School of Aerospace Engineering
Georgia Institute of Technology, Atlanta, GA 30332-0150, USA

Michel Basset, and Gerard Gissinger‡
Ecole Supérieure des Sciences Appliquées pour l'Ingénieur Mulhouse
12, rue des Freres Lumiere, 68093 Mulhouse Cedex, FRANCE.

April 22, 2001

Abstract

In this paper we derive a dynamic friction force model for road/tire interaction for wheeled ground vehicles. The model is based on a similar dynamic friction model for contact developed previously for contact-point friction problems, called the LuGre model [6]. We show that the dynamic LuGre friction model is able to accurately capture velocity and road/surface dependence of the tire friction force. A comparison between the friction forces predicted by our model and experimental data is also provided.

*Corresponding author. Email: canudas@lag.ensieg.inpg.fr
†Email: p.tsiotras@ae.gatech.edu, gte600q@prism.gatech.edu
‡Emails: m.basset@essaim.univ-mulhouse.fr, g.gissinger@essaim.univ-mulhouse.fr

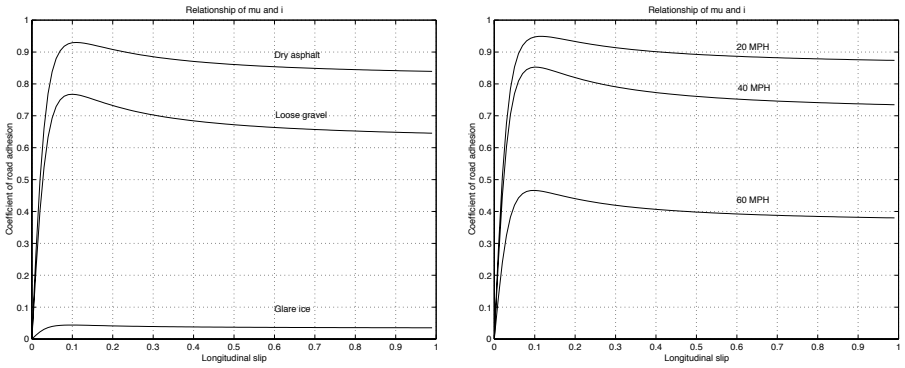

Figure 1: Typical variations of the tire/road friction profiles for different road surface conditions (top), and different vehicle velocities (bottom). Curves given by Harned *et al* in [14].

1 Introduction

The problem of traction control for ground vehicles is of enormous importance to automotive industry. Traction control systems reduce or eliminate excessive slipping or sliding during vehicle acceleration and thus enhance the controllability and maneuverability of the vehicle. Proper traction control design has a paramount effect on safety and handling qualities for passenger vehicles. Traction control aims to achieve maximum torque transfer from the wheel axle to forward acceleration. The friction force at the tire/road interface is the main mechanism for converting wheel angular acceleration (due to the motor torque) to forward acceleration (longitudinal force). Therefore, the study of friction force characteristics at the road/tire interface has received a great deal of attention in the automotive literature. Tire friction model are also important to reproduce for simulion purposes. Active control mechanisms, like the ESP, TCS, ABS, steering control, active suspensions, etc. may be tested and optimized by using vehicle mechanical 3D simulators with a suited tire/road friction models.

A common assumption in most of tire friction models is that the normalized tire friction μ

$$\mu = \frac{F}{F_n} = \frac{\text{Friction force}}{\text{Normal force}}$$

is a nonlinear function of the normalized relative velocity between the road and the tire (slip coefficient s) with a distinct maximum; see Fig. 1. It is also understood that μ depends also on the velocity of the vehicle and road surface conditions, among other factors (see [5] and [14]). The curves shown in Fig. 1 illustrate how these factors influence the shape of μ.

The static model shown in Fig. 1 is derived empirically based solely on steady-state experimental data [14, 2]. Under steady-state conditions, experimental data seem to support the force vs. slip curves of Fig. 1. Nevertheless, the

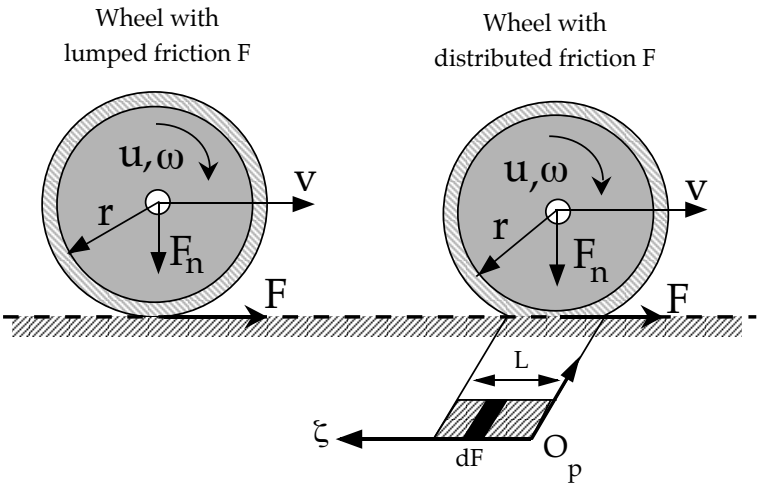

Figure 2: One-wheel system with lumped friction (left), and distributed friction (right)

development of friction force at the tire/road interface is very much a dynamic phenomenon. In other words, the friction force does not reach its steady-state instantaneously, but rather exhibits significant transient behavior which may differ significantly from its steady-state value. Experiments performed in commercial vehicles, have shown that the tire/road forces do not vary along the curves shown Fig. 1, but "jump" from one value to another when these forces are displayed in the $\mu - s$ plane [24]. These variation are most likely to exhibe hysteresis loops, clearly displaying its dynamic nature.

In this paper, we develop new, speed-dependent, dynamic friction models that can be used to describe the tire/road interaction. These models have the advantage that are developed starting from first principles and are based on simple contact (punctual) dynamic friction models [6]. Thus, the parameters entering the models have a physical significance which allows the designer to tune the model parameters based on experimental data. The models are also speed-dependent. This property agrees with experimental observations. A simple parameter in the model can also be used to capture the road surface characteristics. Finally, in opposition to many other static models, our model is shown to be well-defined everywhere (zero rotational or linear vehicle velocities) and hence, is appropriate for any vehicle motion situations (in particular during the braking and acceleration phases), as well as for control law design.

2 Tire/road friction models

In this study we consider a system of the form:

$$m\dot{v} = F \quad (1)$$
$$J\dot{\omega} = -rF + u\,, \quad (2)$$

where m is 1/4 of the vehicle mass and J, r are the inertia and radius of the wheel, respectively. v is the linear velocity, ω is the angular velocity, u is the accelerating (or braking) torque, and F is the tire/road friction force. For the sake of simplicity, only longitudinal motion will be considered. The dynamics of the braking and driving actuators are also neglected.

2.1 Slip/Force maps

The most common tire friction models used in the literature are those of slip/force maps. They are defined as one-to-one (memoryless) maps between the friction F, and the longitudinal slip rate s, defined as:

$$s = \begin{cases} s_b = 1 - \frac{r\omega}{v} & \text{if} \quad v > r\omega, \quad v \neq 0 \quad \text{braking} \\ s_d = 1 - \frac{v}{r\omega} & \text{if} \quad v < r\omega, \quad \omega \neq 0 \quad \text{driving} \end{cases} \quad (3)$$

The slip rate results from the reduction of the effective circumference of the tire (consequence of the tread deformation due to the elasticity of the tire rubber), which implies that the ground velocity will not be equal to $v = r\omega$. The slip rate is defined in the interval $[0, 1]$. When $s = 0$ there is no sliding (pure rolling), whereas $s = 1$ indicates full sliding.

The slip/force models aim at describing the shapes shown in Fig. 1 via static maps $F(s) : s \mapsto F$. They may also depend on the vehicle velocity v, i.e. $F(s, v)$, and vary when the road characteristics change.

One of the most well-known models of this type is Pacejka's model (see, Pacejka and Sharp [20]), also known as the "magic formula". This model has been shown to suitably match experimental data, obtained under particular conditions of constant linear and angular velocity. The Pacejka model has the form

$$F(s) = c_1 \sin(c_2 \arctan(c_3 s - c_4(c_3 s - \arctan(c_3 s)))) \,,$$

where the $c_i's$ are the parameters characterizing this model. These parameters can be identified by matching experimental data, as shown in Bakker *et al.* [2].

The model proposed by Burckhardt [5] for the tire/road friction characteristics is of the form

$$F(s, v) = \left(c_1(1 - e^{-c_2 s}) - c_3 s\right) e^{-c_4 v} \,, \quad (4)$$

where $c_1, \cdots, c_4$ are constants. The normal load at the tire is kept constant in this model. Note also the velocity dependency of this model, seeking to match variations like the one shown in Fig. 1.

Kiencke and Daiss [15] neglect the velocity dependent term in Eq. (4) and approximate the curve by

$$F(s) = K_s \frac{s}{c_1 s^2 + c_2 s + 1}\,, \tag{5}$$

where K_s is the slope of the $F(s)$ versus s curve when $s = 0$ and c_1 and c_2 are properly chosen parameters. Notice that Eq. (5) is only dependent on the slip s. The value of K_s is assumed to be known. Kiencke and Daiss [15] choose a fixed value of about 30^o for it.

Alternative, Burckhardt [4] proposes a simpler three parameters model,

$$F(s) = c_1(1 - e^{-c_2 s}) - c_3 s\,.$$

Since these models are highly nonlinear in the unknown parameters, they are not well adapted to be used for on-line identification. For this reason, simplified models like

$$F(s) = c_1\sqrt{s} - c_2 s$$

are used in connection with a linear recursive identification algorithms, has been proposed in the literature.

A part from the nonlinearity in the unknown parameters, the major limitation of this models seems to steer from the fact that the unknown parameters are not really invariant, they may strongly depend on the tire characteristics (such as compound, tread type, tread depth, inflation pressure, temperature), on the road conditions (such as type of surface, texture, drainage, capacity, temperature, lubricant, i.e. water or snow), and on the vehicle operational conditions (velocity, load), see Pasterkamp and Paceijka [19].

The "Static Friction Models" apply when we have steady state conditions for the linear and angular velocities. This is rarely true in reality, especially when the vehicle goes through continuous successive phases between acceleration and braking.

As an alternative to the static $F(s)$ maps, different forms of dynamic models can be adopted. The so-called "Dynamic Models" attempt to capture the transient behaviour of the tire-road contact forces under time varying velocities conditions. One such model has been proposed by Bliman et al in [3]. In that reference the friction is calculated by solving a differential equation of the following form[1]

$$\begin{aligned} \dot{z} &= |v_r| A z + B v_r \\ F(z, v_r) &= C z + \mathrm{sgn}(v_r) D \end{aligned} \tag{6}$$

The matrix A is required to be Hurwitz of dimension either one or two, with the latter case being more accurate. Another dynamic model that can be used to accurately predict the friction forces during transients is the LuGre friction model [8]. The details of this model are presented in the sections that follow.

[1] In what follows, the upper dot on a signal stands for the partial time-derivative, i.e. $\dot{z}(\zeta, t) = \frac{\partial z}{\partial t}(\zeta, t)$, and $\frac{d}{dt}$ stands for the total time derivative, i.e. $\frac{dz}{dt}(\zeta, t) = \frac{\partial z}{\partial t}(\zeta, t)$

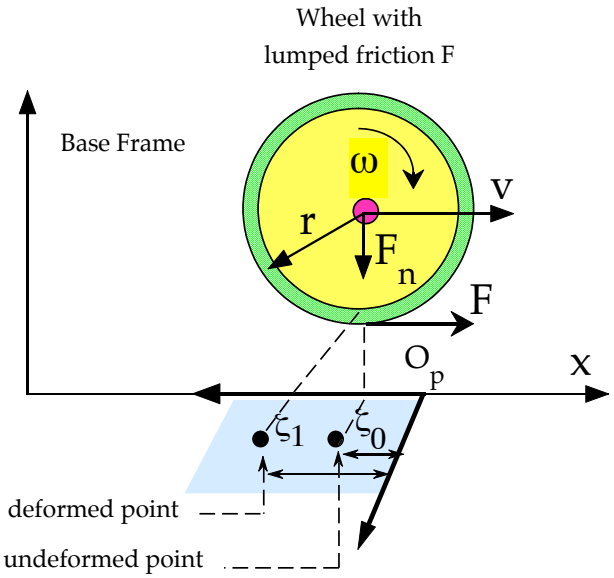

Figure 3: Vie of the contact area with the position of the underformed contact point ζ_0, and the point ζ_1 that deform under longitudinal shear forces.

Dynamic models can be formulated as a lumped or distributed models, as shown in Fig. 2. A *lumped* friction model assumes punctual tire-road friction contact. As a results, the mathematical model describing such a model are ordinary differential equations that can be solved by time integration. Opposed to lumped models, the *distributed* friction assumes the existence of a contact patch with an associated pressure distribution resulting in a partial differential equations, that it need to be solved ith both time and space. This distinction, and the derivation basis of some of these models will be discussed next.

2.2 Lumped dynamic models

Under this consideration, a certain number of dynamic models have been proposed in the literature. We present next two examples of often used dynamic models, and then we introduce an extension of the LuGre model. Nevertheless,it will be show that some of those lumped models are not able to reproduce the steady-state characteristics similar to those of the Paceijka model.

Brush-type models. They are derived from the idealization of a contact point deformation and from kinematic considerations (velocity relations between the points that concern the tire deformations). Its derivation follows semi-empirical considerations, and assumes that the contact forces result from the product of the tire deformation and the tire stiffness.

An example of a two-dimensional model characterizing the lateral force and the aligning momentum, can be found in [17]. A brush model for the longitudinal tire dynamic has been derived in [9, 1].

The proposed model for the longitudinal dynamics, is derived by defining the normalized longitudinal slip z as:

$$z = \frac{\zeta_1 - \zeta_0}{\zeta_1}$$

where ζ_1 locates a hypothetical element which follows the road, and ζ_0 locates a hypothetical element which in undeformed under longitudinal shear forces, as shown in Fig. 3. Differentiating z with respect to time, and noticing that $\dot{\zeta_0} = r\omega$, $\dot{\zeta_1} = v$, we get (for simplicity, we only discuss the case of $v > 0$):

$$\frac{1}{\sigma}\dot{z} = v_r - |v|z \tag{7}$$

$$F = h(z) = kz \tag{8}$$

where v is the linear velocity, $v_r = r\omega - v$ is the relative velocity, and the contact force F is defined by the function $h(z)$ that defined in general the stationary slip characteristics. In the simplest case, $h(z)$ is given by a linear relationship between the longitudinal slip and the tire (linear) stiffness k. The constant[2] $1/\sigma = \zeta_1$ is called the relaxation length, which can be defined as the distance required to reach the steady-state value of F

$$F_{ss} = h(z_{ss}) = kz_{ss} = k\frac{r\omega - v}{v}\text{sign}(v) = ks$$

after a steep change of the slip longitudinal velocity, $s = v_r/v = (r\omega - v)/v$. The role of the relaxation length $1/\sigma$ in the equation (7), can be better understood by rewriting this equation in terms of the spatial coordinate η:

$$\eta(t) = \int_0^t |v(\tau)|d\tau$$

rather than as a time-differential equation, i.e.

$$\frac{1}{\sigma}\frac{dz}{dt} = \frac{1}{\sigma}\frac{dz}{d\eta}\frac{d\eta}{dt} = v_r - |v|z \tag{9}$$

$$\frac{1}{\sigma}\frac{dz}{d\eta} = -z + \frac{v_r}{|v|} = -z + s \tag{10}$$

where the last equality results form the consideration on that $v > 0$. Equation (10) can thus be seen as a first order spatial equation with the sliding velocity s as its input. It becomes clear thus that σ represent the *spatial* constant of this equation.

[2]When following the derivation of this model, it is not clear under which conditions ζ_1 can be considered constant. Indeed, in certain works, the relaxation length has been make a function of the slip deformation, see [17]

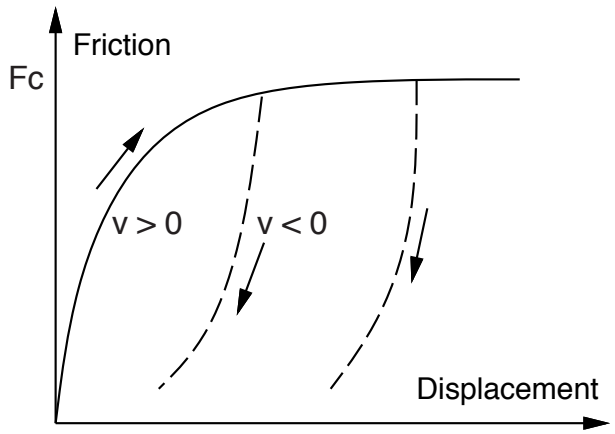

Figure 4: Friction force as a function of displacement fro the Dahl's model.

As pointed out in [9], the model work well for high speeds, but it generates lightly damped oscillations at low speeds. The reason is that at quasi-steady-state regime, z is close to its steady-state value ($z \approx s$) , and that friction F is dominated by its spring-like behaviour ($F \approx kz$), resulting in a lightly damped mechanical system. As it will be show later, during the presentation of the LuGre model, the oscillations can be cancelled by introducing an additional damping term at the output F. Others consideration are necessary to make this model consistent with all possible changes in the velocity sign. [9] provides a twelve-step algorithm for implementing this model in simulations.

The Dahl model The Dahl model [10] was developed for the purpose of simulating control systems with friction. The starting point for Dahl's model is the stress-strain curve in classical solid mechanics [21] and [22] (Fig. 4). When subject to stress, the friction force increases gradually until rupture occurs. Dahl modeled the stress-strain curve by a differential equation. Let x_r be the relative displacement, $v_r = \frac{dx_r}{dt}$ the relative velocity, F the friction force, and F_C the maximal friction force (Coulomb force). Then the Dahl's model has the form:

$$\frac{dF}{dx} = \sigma_0 \left(1 - \frac{F}{F_C}\text{sign}(v_r)\right)^{\alpha} \tag{11}$$

where σ_0 is the stiffness coefficient α is a parameter that determines the shape of the stress-strain curve. The value $\alpha = 1$ is most commonly used. Higher values will give a stress-strain curve with sharper bend. The friction force $|F|$ will be never be larger than F_C if its initial value is such that $|F(0)| < F_C$. When integrating 11, it can be observed a monotonic growing of $F(t)$ after step changes on v_r. Therefore the Dahl's model canot exhibe a maximum peaking, as the Paceika's behaviour suggest.

It is also important to remark that in this model the friction model is only a function of the displacement and the sign of the relative velocity. This implies that the evolution of the friction force in the $F-x$ plane will only depend on the sign of the velocity, but not on the magnitude of v_r. This property is called rate-independent, and it makes possible the theory of hysteresis operators to be used.

To obtain a time domain model Dahl observed that:

$$\frac{dF}{dt} = \frac{dF}{dx}\frac{dx}{dt} = \frac{dF}{dx}v_r = \sigma_0 \left(1 - \frac{F}{F_C}\text{sign}(v_r)\right)^{\alpha} v_r \tag{12}$$

For the case $\alpha = 1$, the Dahl model (12) can be written as

$$\frac{dF}{dt} = \sigma_0(v_r - \frac{F}{F_C}|v_r|) \tag{13}$$

or in it state model description:

$$\frac{dz}{dt} = v_r - \sigma_0 \frac{z}{F_C}|v_r| \tag{14}$$

$$F = \sigma_0 z \tag{15}$$

with z being the relative displacement. Note the different in the interpretation of z in the brush model where it represent the *normalized* relative displacement.

Introducing the *relative* length distance η_r, as:

$$\eta_r(t) = \int_0^t |v_r(\tau)|d\tau$$

The Dahl models becomes

$$\frac{1}{\sigma_0}\frac{dF}{d\eta_r} = -\frac{1}{F_c}F + \text{sign}(s) \tag{16}$$

In this coordinates, the Dahl model behaves as a linear space invariant system with the sign of the longitudinal slip velocity as its input. The motion in the $F-\eta_r$ plane is thus independent of the magnitude of the slip velocity.

Comparison between the Brush and the Dahl model. It is also instructive to compare the brush model with the Dahl model. First note that the steady-state values for each models are:

$$F_{ss}^{brush} = ks, \qquad F_{ss}^{Dahl} = F_C\text{sign}(s)$$

Since $|s| \leq 1$, then k and and F_C represent the maximum values that the friction can take. In steady state, the brush model predicts a linear behaviour with respect to s, whereas the Dahl model predicts a discontinuous form with values in the set $[-F_C, F_C]$.

In the neighborhood of $v_r = 0$, both models predict similar linearized pre-sliding behaviour (spring like),

$$F_{ss}^{brush} \approx k\sigma\eta_r, \tag{17}$$
$$F_{ss}^{Dahl} \approx \sigma_0\eta_r \tag{18}$$

but there are some differences when comparing the complet dynamic equations of both models. Consider the particular form $h(z) = kz$ in the equation (8), then the spatial representations of both models in the η, and the η_r coordinates are given as:

$$\frac{1}{\sigma_0}\frac{dF^{Dahl}}{d\eta_r} = -\frac{1}{F_c}F^{Dahl} + \text{sign}(s) \tag{19}$$
$$\frac{1}{k\sigma}\frac{dF^{brush}}{d\eta} = -\frac{1}{k}F^{brush} + \text{sign}(s) \tag{20}$$

Let $F_c = k$, and $\sigma_0 = k\sigma$, then both models looks similar. Note however that they are defined in a different coordinates, which change the interpretation that may be given to the relaxation length constant: $F_c\sigma_0$ describes the relaxation length of the Dahl's model with respect to the *relative* (sliding) distance, whereas $1/\sigma$ represents the relaxation length of the brush model defined with respect to the *absolute* (total) traveled longitudinal distance.

Note also that the two models above do not exhibit a maximum for values $|s| < 1$, as the Pacejka's does. However, the brush model can be modified by redefining the function $h(z)$ so as to produce a steady-state behaviour similar to the one depicted by the Magic formula [1].

Lumped-LuGre model The LuGre model[3] is an extension of the Dahl's model that include the Stribeck effect (see, [6]). This model will be used as a basis for further developments for the final model proposed in this paper. The Lumped-LuGre model as proposed in [8], and [7] is given as:

$$\dot{z} = v_r - \frac{\sigma_0|v_r|}{g(v_r)}z \tag{21}$$
$$F = (\sigma_0 z + \sigma_1\dot{z} + \sigma_2 v_r)\, F_n \tag{22}$$

with,

$$g(v_r) = \mu_C + (\mu_S - \mu_C)e^{-|v_r/v_s|^{\frac{1}{2}}}$$

where σ_0 is the rubber longitudinal lumped stiffness, σ_1 the rubber longitudinal lumped damping, σ_2 the viscous relative damping, μ_C the normalized Coulomb friction, μ_S the normalized Static friction,($\mu_C \leq \mu_S \in [0,1]$), v_S the Stribeck

[3]This model differs from the one in [6] in the way that the function $g(v)$ is defined. Here we propose to use the term $e^{-|v_r/v_s|^{\frac{1}{2}}}$ instead the term $e^{-(v_r/v_s)^2}$ as in the LuGre point-contact model in order to better match the pseudo-stationary characteristic of this model (map $s \mapsto F(s)$) with the shape of the Pacejka's model, as it will be shown later.

relative velocity, F_n the normal force, $v_r = (r\omega - v)$ the relative velocity, and z the internal friction state.

In opposition to the Dahl's model, the lumped LuGre model does exhibit a maximum for values $|s| < 1$, but it still displaying discontinuous steady-state characteristics, at zero relative velocity. Nevertheless, by letting the internal bristle deflection z depends on both the time and the contact position ζ, it is possible to show that the model in that case will have the suited stead-state properties.

2.3 Distributed models

Distributed models assume the existence of an area of contact (or patch) between the tire and the road, as shown in Fig. 2. This patch represents the projection of the part of the tire that is in contact with the road. With the contact patch is associated a frame O_p, with ζ-axis along the length of the patch in the direction of the tire rotation. The patch length is L.

Distributed dynamical models, have been studied previously, for example, in the works of Bliman *et al.* [3]. In these kinds of models, the contact patch area is discretized to a series of elements, and the microscopic deformation effects are studied in detail. In particular, Bliman *at al.* characterize the elastic and Coulomb friction forces at each point of the contact patch, and they give the aggregate effect of these distributed forces by integrating over the whole patch area. They propose a second order rate-independent model (similar to Dahl's model), and show that, under constant v and ω, there exists a choice of parameters that closely match a curve similar to the one characterizing the magic formula.

One can also extend the point friction model (21)-(22) to a distributed friction model along the patch by letting $z(\zeta, t)$ denote the friction state (deflection) of the bristle/patch element located at the point ζ along the patch at a certain time t. The model (21)-(22) can now be written as:

$$\frac{d\,z}{dt}(\zeta, t) = v_r - \frac{\sigma_0 |v_r|}{g(v_r)}\, z \tag{23}$$

$$F = \int_0^L dF(\zeta, t)\, d\zeta\,, \tag{24}$$

with $g(v_r)$ defined as before and

$$dF(\zeta, t) = \left(\sigma_0\, z + \sigma_1 \frac{\partial z}{\partial t} + \sigma_2 v_r\right) f_n(\zeta)\,,$$

where, dF is the differential friction force (force per unit length), $f_n(\zeta)$ is the normal force distribution, $v_r = (r\omega - v)$ is the relative velocity of each bristle in contact. The model assumes that the contact velocity of each differential state element is equal to v_r.

Noting that $\dot{\zeta} = \frac{\partial \zeta}{\partial t} = |r\omega|$ (the frame origin changes location when the wheel velocity reverses: $\dot{\zeta} = r\omega$, for $\omega > 0$, and $\dot{\zeta} = -r\omega$, for $\omega < 0$), and that

$\frac{dz}{dt}(\zeta,t) = \frac{\partial z}{\partial \zeta}\frac{\partial \zeta}{\partial t} + \frac{\partial z}{\partial t}$, we have that equation (23) describes a partial differential equation (PDE), i.e.

$$\frac{\partial z}{\partial \zeta}(\zeta,t)\,|r\omega| + \frac{\partial z}{\partial t}(\zeta,t) = v_r - \frac{\sigma_0|v_r|}{g(v_r)}\,z(\zeta,t) \tag{25}$$

that should be solved in both time and space. More details on the model derivation basis are given in the Appendix.

Steady-state characteristics. The (time) steady-state characteristics of the model (23)-(24) are obtained under $\frac{\partial z}{\partial \zeta}(\zeta,t) \equiv 0$ and by setting the velocities v and ω constants. Enforcing this conditions in (25) results in

$$\frac{\partial z(\zeta,t)}{\partial \zeta} = \frac{1}{|\omega r|}\left(v_r - \frac{\sigma_0|v_r|}{g(v_r)}z(\zeta,t)\right) \tag{26}$$

At steady-state, v,ω (and hence v_r) are constant, and (26) can be integrated along the patch with the boundary condition $z(0,t) = 0$. A simple calculation shows that

$$z_{ss}(\zeta) \;=\; \mathrm{sgn}(v_r)\frac{g(v_r)}{\sigma_0}(1 - e^{-\frac{\sigma_0}{g(v_r)}\left|\frac{v_r}{\omega r}\right|\zeta}) = c_2(1 - e^{c_1\zeta}) \tag{27}$$

where

$$c_1 = -\frac{\sigma_0}{g(v_r)}\left|\frac{v_r}{\omega r}\right|, \qquad c_2 = \mathrm{sgn}(v_r)\frac{g(v_r)}{\sigma_0} \tag{28}$$

Note that when $\omega = 0$, the distributed model, and hence the steady-state expression (27) collapses into the one predicted by the standard punctual contact LuGre model.

In order to calculate the steady-state value of the total friction force from (57), i.e.

$$F_{ss} = \int_0^L (\sigma_0 z_{ss}(\zeta) + \sigma_2 v_r) f_n(\zeta) d\zeta \tag{29}$$

we need to assume a distribution for the normal force $f_n(\zeta)$. A Typical form of the normal force distribution reported in the literature [23, 18, 13, 12], is shown in Fig. 5. However, for seek of simplicity, other forms can be adopted. Some examples are:

- *Constant norm distribution.* A simple result can be derived if we assume uniform load distribution, as done in [8] and [11]. For uniform normal load

  $$f_n(\zeta) = \frac{F_n}{L} \tag{30}$$

  and one obtains,

  $$F_{ss} = \left(\mathrm{sgn}(v_r)g(v_r)\Big[1 - \frac{Z}{L}(1 - e^{-L/Z})\Big] + \sigma_2 v_r\right) F_n \tag{31}$$

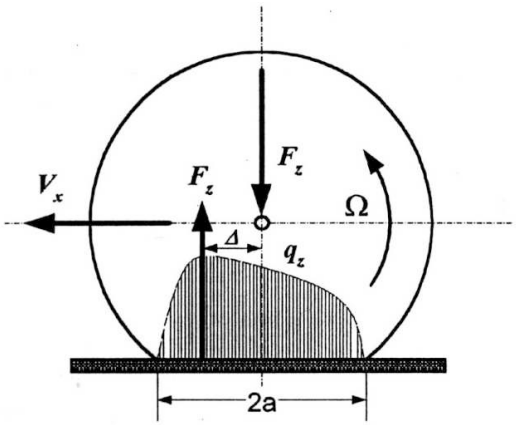

Figure 5: Typical normal load distribution along the patch; from [?].

where

$$Z = \left|\frac{\omega r}{v_r}\right| \frac{g(v_r)}{\sigma_0} \tag{32}$$

- *Exponentially decaying distribution.*

$$f_n(\zeta) = a^{(\frac{\zeta}{L})} f_{n0}, \qquad 0 < a \leq 1 \tag{33}$$

where $f_n(0) = f_{n0}$ denotes the distributed normal load for $\zeta = 0$. This particular choice will become clear later on, when we reduce the infinite dimension distributed model to a simple lumped one having one state variable. Moreover, for $a < 1$ we have a decreasing function of f_n. With this choice one obtains

$$F_{ss} = \sigma_0 c_2 k_1 \Big(e^{\ln a} - k_2 e^{(\ln a + CL)} - 1 + k_2 \Big) + \sigma_2 v_r k_1 (a - 1) \tag{34}$$

where

$$k_1 = \frac{f_{n0} L}{\ln a} \qquad \text{and} \qquad k_2 = \frac{\ln a}{\ln a + CL}$$

Details of this calculations are in the Appendix. The value of f_{n0} can be computed from a, L and the total normal load F_n acting on the wheel shaft. That is,

$$F_n \;=\; \int_0^L f_n(\zeta) d\zeta = \int_0^L a^{\frac{\zeta}{L}} f_{n0} d\zeta = f_{n0} \Big[\frac{L}{\ln a} a^{\frac{\zeta}{L}} \Big]_0^L$$

$$= \frac{f_{n0}L}{\ln a}(a-1)$$

which yields,

$$f_{n0} = F_n \frac{\ln a}{(a-1)L} \tag{35}$$

- *Distributions with zero boundary conditions.* As shown in Fig. 5, the more realistic force distributions have, by continuity, zero boundary values. Several forms can be proposed. Some possible examples are:

$$f_n(\zeta) = \frac{3}{2}F_n\left[1 - \left(\frac{\zeta - L/2}{L/2}\right)^2\right] \tag{36}$$

or,

$$f_n(\zeta) = F_n \sin(\pi\zeta/L) \tag{37}$$

or,

$$f_n(\zeta) = F_n \exp^{-\gamma\zeta} \sin(\pi\zeta/L) \tag{38}$$

Relation with the magic formula. The previously derived steady-state expressions, depend on both v and ω. They can also be expressed as a function of s and either v or ω. For example, for the constant distribution case, we have that $F_{ss}(s)$, can be rewritten as:

- *Driving case.*

$$F_d(s) = \mathrm{sgn}(v_r)F_n g(s)\left(1 + \frac{g(s)}{\sigma_0 L|s|}(e^{-\frac{\sigma_0 L|s|}{g(s)}} - 1)\right) + F_n\sigma_2 r\omega s \tag{39}$$

with $g(s) = \mu_C + (\mu_S - \mu_C)\, e^{-|r\omega s/v_s|^{\frac{1}{2}}}$, for some constant ω, and $s_d = s \in [0,1]$.

- *Braking case.* Noticing that the following relations hold between the braking s_b and the driving s_d sliding velocity definitions:

$$r\omega s_d = v s_b, \qquad s_d = \frac{s_b}{s_b - 1}$$

the braking case writes as

$$F_b(s) = \mathrm{sgn}(v_r)F_n g(s)\left(1 + \frac{g(s)|1-s|}{\sigma_0 L|s|}(e^{-\frac{\sigma_0 L|s|}{g(s)|1-s|}} - 1)\right) + F_n\sigma_2 \tag{40}$$

with $g(s) = \mu_C + (\mu_S - \mu_C)\, e^{-|vs/v_s|^{\frac{1}{2}}}$, for some constant v, and $s_b = \in [0,1]$.

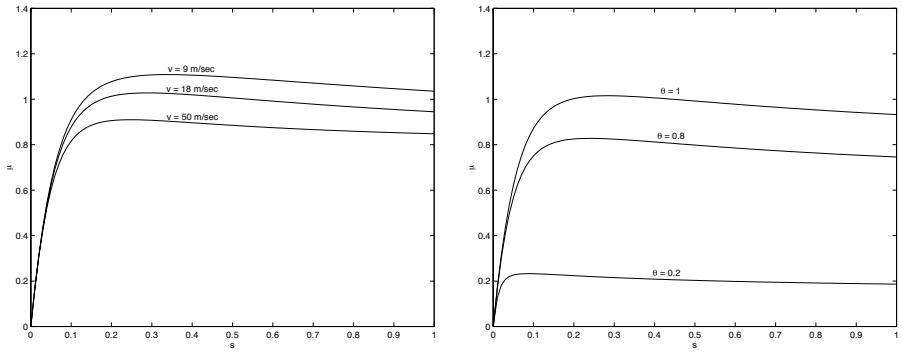

Figure 6: Static view of the distributed LuGre model (braking case) with uniform force distribution (Expression of F_b) under: (a)-left different values for v, (b)-right different values for θ with $v = 20m/s = 72Km/h$. These curves show the normalized friction $\mu = F(s)/F_n$, as a function of the slip rate s.

Remark: Note that the above expressions depends not only on s, but either on v or ω depending the considered case. Therefore plots of F versus s can only be obtained for a specified (constant) velocity. The velocity-dependency of the steady-state curves is also present in the data found in the literature. Nevertheless, it should be stressed the impossibility reproduce such a curves form experimental data obtained from standard vehicles where v and ω cannot be independently controlled. For that, specially design equipment is needed. Fig. 6-(a) shows the steady-state characteristics for the braking case, with the data given in Table 1.

Parameter	**Value**	**Units**
σ_0	181.54	[1/m]
σ_2	0.0018	[s/m]
μ_C	0.8	[-]
μ_S	1.55	[-]
v_s	6.57	[m/s]
L	0.2	[m]

Table 1: Data used for the plot shown in Fig. 6

Dependency on road conditions. The level of tire/road adhesion, can be modeled by introducing a multiplicative parameter θ in the function $g(v_r)$. To this aim, we substitute $g(v_r)$ by

$$\tilde{g}(v_r) = \theta g(v_r)\,,$$

where $g(v_r)$ is the nominal known function as given before. Computation of the function $F(s,\theta)$, from Eq. (40) as a function of θ, gives the curves shown in

Fig. 6-(b). These curves match reasonably well the experimental data shown in Fig. 1-(a), for different coefficients of road adhesion using the parameters shown in Table 1. Hence, the parameter θ, can suitably describes the changes in the road characteristics.

Note that the steady-state representation of Eq. (39) can be used to identify most of the model parameters by feeding this model to experimental data. These parameters can also be used in the simpler mean lumped model, which can be shown to suitably approximate the solution of the PDE described by Eqs. (23) and (24). This approximation is discussed next.

2.4 From distributed to lumped mean models

It is clear that the distributed model captures reality better than the lumped, point contact model. It is also clear that in order to use the distributed model for control purposes it is necessary to choose a discrete number of states to describe the dynamics for each tire. This has the disadvantage that a possibly large number of states is required to describe the friction generated at each tire. Alternatively, one could define a *mean friction state* $\bar{z}$ for each tire and then derive an *ordinary differential equation* for $\bar{z}$. To this end, let us define

$$\bar{z}(t) \equiv \frac{1}{F_n}\int_0^L z(\zeta,t) f_n(\zeta) d\zeta \tag{41}$$

where F_n is given by

$$F_n = \int_0^L f_n(\zeta)\, d\zeta$$

Thus,

$$\dot{\bar{z}}(t) = \frac{1}{F_n}\int_0^L \frac{\partial z}{\partial t}(\zeta,t) f_n(\zeta) d\zeta \tag{42}$$

From (54) we get

$$\begin{aligned}
\dot{\bar{z}}(t) &= \frac{1}{F_n}\int_0^L \Big(v_r - \frac{\sigma_0|v_r|}{g} z(\zeta,t) - \frac{\partial z(\zeta,t)}{\partial \zeta}|\omega r|\Big) f_n(\zeta) d\zeta \\
&= v_r - \frac{\sigma_0|v_r|}{g}\bar{z}(t) - \frac{|\omega r|}{F_n}\int_0^L \frac{\partial z(\zeta,t)}{\partial \zeta} f_n(\zeta) d\zeta \\
&= v_r - \frac{\sigma_0|v_r|}{g}\bar{z}(t) - \frac{|\omega r|}{F_n}\Big[z(\zeta,t) f_n(\zeta)\Big]_0^L + \frac{|\omega r|}{F_n}\int_0^L z(\zeta,t)\frac{\partial f_n(\zeta)}{\partial \zeta} d\zeta
\end{aligned}$$

The term in the square brackets describes the influence of the boundary conditions, whereas the integral term accounts for the particular form of the force distribution.

From another hand, we have from (24),

$$\begin{aligned}
F(t) &= \int_0^L \left(\sigma_0\, z(\zeta,t) + \sigma_1 \frac{\partial z}{\partial t}(\zeta,t) + \sigma_2 v_r\right) f_n(\zeta)\, d\zeta \\
&= \left(\sigma_0 \bar{z}(t) + \sigma_1 \dot{\bar{z}}(t) + \sigma_2 v_r\right) F_n
\end{aligned}$$

As a general goal, one may wish to introduce distributions, that lead to the following form (mean lumped LuGre model),

$$\dot{\bar{z}}(t) = v_r - \frac{\sigma_0|v_r|}{g}\bar{z}(t) - \kappa(\cdot)|\omega r|\bar{z}(t) \tag{43}$$

$$F(t) = (\sigma_0\bar{z}(t) + \sigma_1\dot{\bar{z}}(t) + \sigma_2 v_r)\, F_n \tag{44}$$

where κ is defined as:

$$\kappa(\cdot)\bar{z} = \frac{1}{F_n}\left\{\Big[z(\zeta,t)f_n(\zeta)\Big]_0^L - \int_0^L z(\zeta,t)\frac{\partial f_n(\zeta)}{\partial\zeta}d\zeta\right\} \tag{45}$$

and F_n as above. When comparing this model with the punctual LuGre one (21)-(22), it is clear that κ capture its distributed nature. It may also expected that $\kappa > 0$, so that the map $v_r(t) \mapsto F(t)$ preserve the similar passivity properties that the punctual model.

Note also that according to the hypothesis taking on the force distribution form, different expressions for the mean model can be developed: κ may then become a constant, an explicit or an implicit function of $\bar{z}$. We study some of these forms next.

Exponentially decaying distributions. Now, assuming (33) as well as $z(0,t) = 0$ we get

$$\begin{aligned}\kappa(\cdot)\bar{z} &= \frac{1}{F_n}\Big[z(\zeta,t)a^{\zeta/L}f_{n0}\Big]_0^L - \frac{1}{F_n}\int_0^L z(\zeta,t)\frac{\ln a}{L}a^{\zeta/L}f_{n0}\,d\zeta \\ &= \frac{1}{F_n}z(L,t)af_{n0} - \frac{\ln a}{L}\,\bar{z}(t)\end{aligned} \tag{46}$$

Next, recall that we require $a \leq 1$. For very small values of a it is possible to ignore the term containing $z(L,t)$ in the equation above, and approximate $\kappa(\cdot)$ by a constant

$$\kappa = -\frac{\ln a}{L}, \quad \text{with} \quad 0 < a < 1 \tag{47}$$

Uniform normal distribution. The case of the uniform normal distribution can be viewed as a special case of (33) with $a = 1$. In this case $f_n(\zeta) = f_{n0} = F_n/L$ and we obtain the following expression

$$\kappa(\cdot)\bar{z} = \frac{1}{F_n}z(L,t)f_{n0} = \frac{1}{L}z(L,t) \tag{48}$$

Deur [11] proposed that the boundary condition for the last element $z(L,t)$ be approximated by an expression afine to the mean deflection $\bar{z}$, i.e.

$$z(L,t) \approx \kappa_0(\cdot)\bar{z} \tag{49}$$

resulting in the relation,

$$\kappa = \frac{\kappa_0}{L} \tag{50}$$

The function $\kappa_0(\cdot)$ in (49) is chosen in [11] so that the steady state solutions of the total friction force for the mean lumped (43)-(44), and the one of the distributed model (expression (31)are the same. This results in the following expression for κ_0

$$\kappa_0 = \kappa_0(Z) = \frac{1 - e^{-L/Z}}{1 - \frac{Z}{L}(1 - e^{-L/Z})} \tag{51}$$

In [11] it is also shown that, κ_0 belongs to the range $\in [1, 2]$, but that a constant value for $\kappa_0 \in [1, 2]$ can be chosen, while making the steady states of the distributed and lumped models only slightly different, as it is shown in Fig. 7

Next, we present several plots of the steady state of the distributed model with uniform and non-uniform normal load distribution, along with the steady state plots of both lumped models, and for different values of κ and a. We use the same parameters $\sigma_0, \sigma_2, \mu_s, \mu_c$ and v_s for both models. In particular we choose the values shown in Table 2. All steady state plots were made for

Parameter	Value
σ_0	200 m^{-1}
σ_2	0 sec /m
μ_c	0.5
μ_s	0.9
v_s	12.5 m/ sec

Table 2: Common Parameters

constant vehicle velocity $v = 20\mathrm{m/\,sec}$ and patch length $L = 0.2\mathrm{m}$.

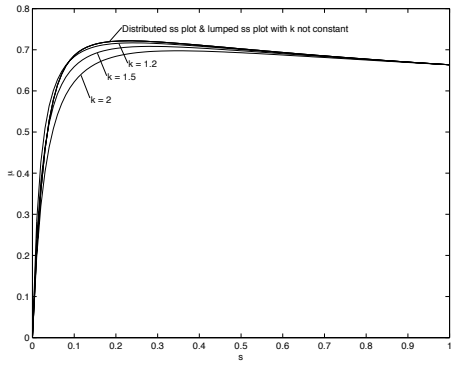

Figure 7: Steady state plots assuming normal load distribution using the approximation from [11].

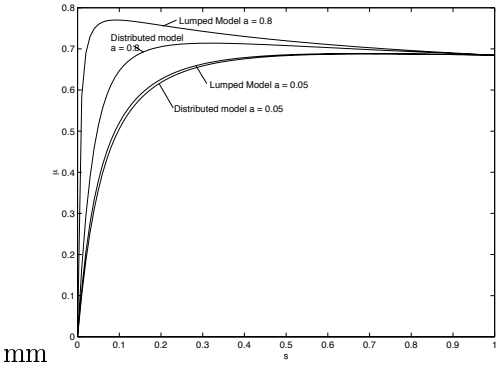

mm

Figure 8: Steady state plots assuming the load distribution given in (33).

3 Experimental Results

In this section we briefly present the measurements collected during three brakings of the a vehicle under the same vehicle operational and road conditions. We will be using this data to identify the parameters of the mean lumped LuGre model. We then use these parameter and validate the dynamic friction model by comparing the time histories of the friction force predicted by the proposed extension of the LuGre model with the friction force from the three experiments.

Testbed car description The "BASIL" car is a laboratory car based on a Renault Mégane 110 Kw. It has been equipped with several different sensors to study the behaviour of the vehicle during the breaking and traction phases. These sensors are (see Fig. 9):

- an optic cross-correlation sensor to measure the transverse and longitudinal vehicle velocities,
- a basic inertial unit with a piezoelectric vibrating gyroscope to measure the yaw rate and another one to measure the roll velocity,
- a magnetic compass for the direction, and
- two acceleration sensors to measure the longitudinal and lateral accelerations,
- the ABS-system is used to derive, troughout a suitable signal processing, the wheels' velocities ω_i,
- a DGPS system has been used to locate the vehicle and compute its trajectory with great accuracy (less than one centimeter). [Michel: en quoi cette inforest utile; pour calculer v ?],
- specific-purpose sensors (not described here) have been used to measure the throttle angle and collector pressure (driver activity) [Michel a quoi servent, dans notre cas, ces measures ?].

For this application, a Kistler wheel force transducer has been installed in [Michel: a la place de, ou dans la place de ?] place of the standard right rim to measure the dynamic forces and moments acting between the road and the vehicle. Its weight must be [Michel most be or is ?] small, considering the unsprung mass.

This sensor gives the complete wrench in real time, namely forces F_x, F_y, F_z and moment M_z. These variables are shown in Fig. 10. The complete equipped vehicle is presented with all the measurement parameters in Fig. 9.

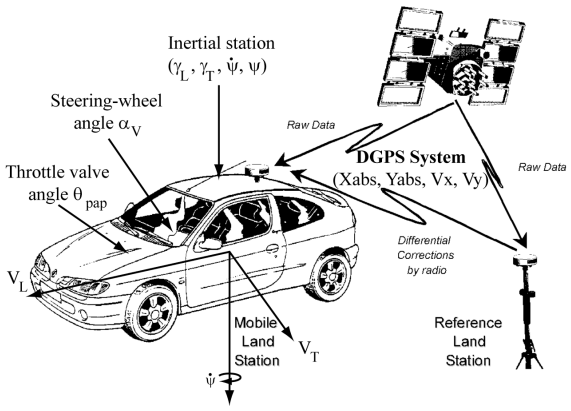

Figure 9: Sensors and measurement parameters.

Trials description. For safety reasons, the trials were carried out on a straight test track under dry weather conditions. The intended driving situations were highlighted and analysed through a set of experiments with the equipped vehicle called BASIL. After an accelerating phase, the vehicle speed was maintained constant at a pre-defined speed. Then, in order to match iso [Michel: what are the iso condition, please describe] conditions and small values of forces F_x and F_z before the braking phase, the test driver released the clutch for a few seconds. The speed of the vehicle decreased slightly. Then, the test driver start the braking phase and strongly brakes until the grip limit of the front wheels was reached. Finally, he released the brake pedal and accelerated again to repeat the same sequence. Three braking phases were performed and stored in file.

Collected data The collected data obtained throughout experiments are shown in figures Fig. **??**, and Fig. **??**. Fig. **??** shows the measurements of the braking pressure, the longitudinal speed of the vehicle and the RFW [Michel: what mean ?] velocity, for three braking phases. Fig. **??** shows the different measurements of forces F_x, F_y and F_z, and the lateral acceleration g_t. The values of F_y and g_t clearly show the lateral excitation of the vehicle during the braking phases, due to geometrical aspects of the suspension system. However

Parameter identification and lumped-LuGre model validation The experimental data consists of measurements of the longitudinal slip s, friction coefficient μ, and linear velocity v. We also know the sampling frequency of the measurements which allows us to re-construct the time vector.

First, we compare the steady state solution of the distributed dynamical model at the mean velocity of the experiments with the friction coefficient μ given by the experiments. We plots the corresponding μ vs. slip curves and

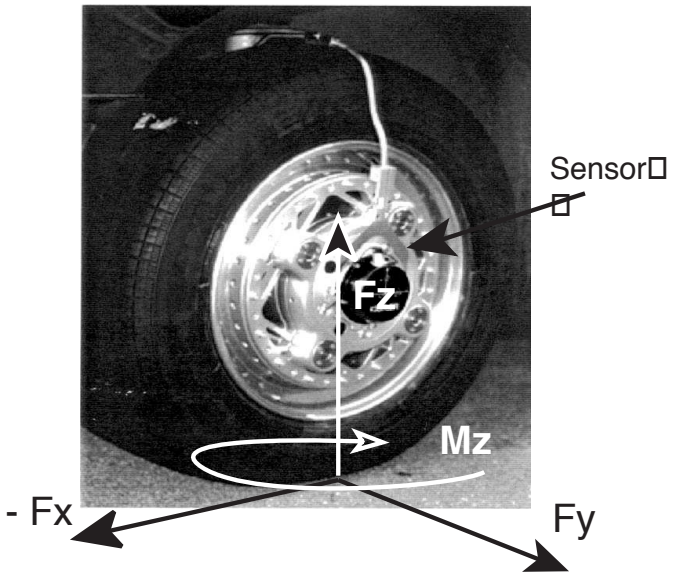

Figure 10: View of the equipped wheel with the Kistler sensor and variables measured.

determine the parameters of the model ($\sigma_0, \sigma_2, \mu_s, \mu_c$ and v_s). We then compare the time histories of the friction force given by our the model with the ones given by the experiments to determine the rest of the parameters (e.g., σ_1).We used the $s - \mu$ plot of only one experiment (Braking #2) to identify the parameters for the steady state solution.

In order to identify the model parameters we use an optimization algorithm of MATLAB and fit the steady state solution of the distributed model to the μ - s plot data of Braking #2. For simplicity, when running the optimization algorithm we used a fixed value for v_s and a. The patch length was chosen as $L = 0.2$m and the total normal force was chosen as $F_n = 3000$ N. This was done for uniform normal load distribution with $\kappa = 1.2$ (case (i)), and with varying κ (case (ii)). The results for the normal load distribution in (33) and $a = 0.05$ are also presented, for comparison (case (iii)).

The results of the identification are shown below.

The normal load distribution at the contact patch for case (iii) is shown in Fig. **??**

The comparison between the experimental results and the simulation results using the LuGre dynamic friction model for the three cases are shown in Figs. **??**-**??**.

Parameter	Value
σ_0	m^{-1}
σ_1	m^{-1}
σ_2	$\mathrm{sec}\,/\mathrm{m}$
μ_c	
μ_s	
v_s	m/sec

Parameter	Value
σ_0	$178\ \mathrm{m}^{-1}$
σ_1	$1\ \mathrm{m}^{-1}$
σ_2	$0\ \mathrm{sec}\,/\mathrm{m}$
μ_c	0.8
μ_s	1.5
v_s	$5.5\ \mathrm{m}/\mathrm{sec}$

Parameter	Value
σ_0	m^{-1}
σ_1	m^{-1}
σ_2	$\mathrm{sec}\,/\mathrm{m}$
μ_c	
μ_s	
v_s	m/sec

Table 3: Data used for the plots concerning the cases (i) left, (ii)-center, and (iii)-right.

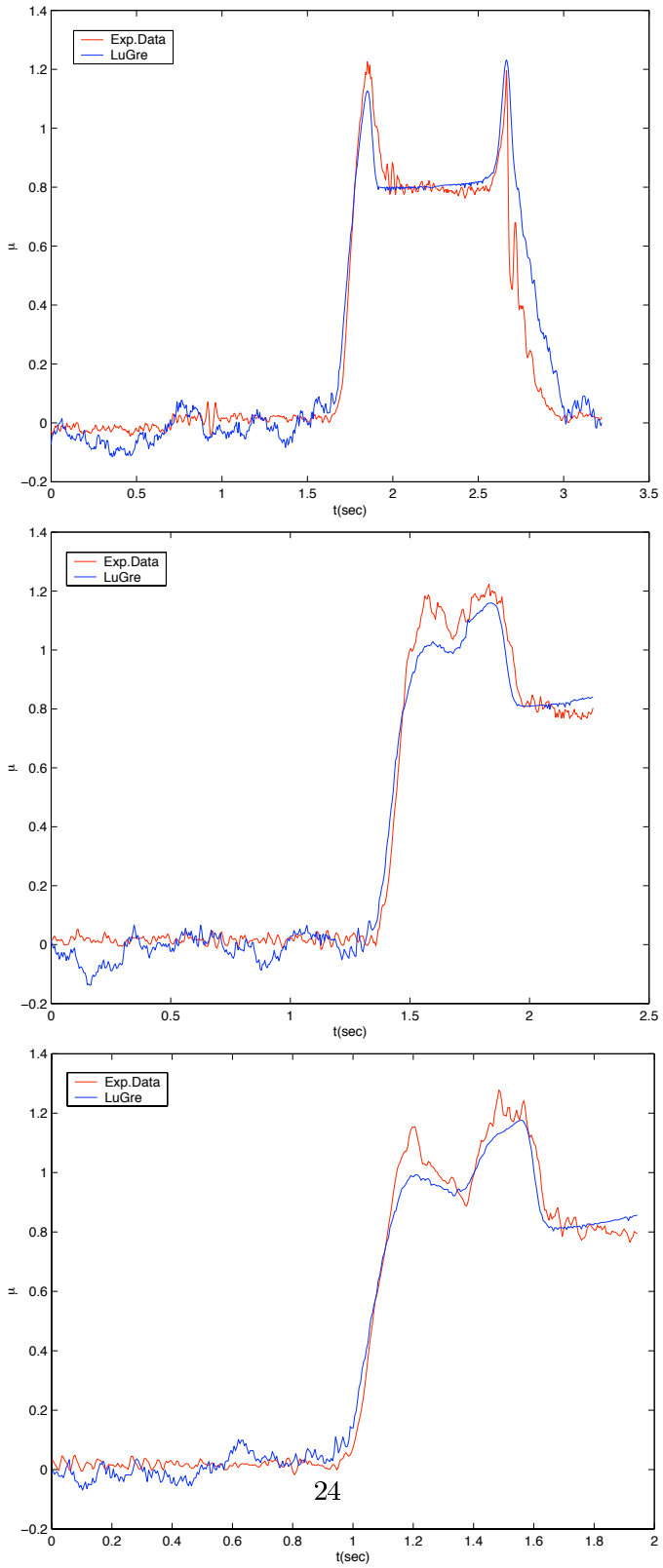

Figure 11: case (ii): varying κ.

4 Conclusions

Appendix

Details of the distribution model derivation. Let $z(\zeta, t)$ denote the friction state (deflection) of the bristle/patch element located at the point ζ along the patch at a certain time t and consider the total deflection of this element between two time instances t and $t + dt$. Since the time interval dt the element has moved to the location $\zeta + d\zeta$, and using (21)-(22), we have that (see also Fig. 12)

$$z(\zeta + d\zeta, t + dt) - z(\zeta, t) = (v_r - \frac{\sigma_0 |v_r|}{g(v_r)} z(\zeta, t))\, dt \tag{52}$$

Expand $z(\zeta + d\zeta, t + dt)$ as follows,

$$z(\zeta + d\zeta, t + dt) = z(\zeta, t) + \frac{\partial z}{\partial \zeta} d\zeta + \frac{\partial z}{\partial t} dt + \cdots$$

and substitute in (52). Dividing both sides by dt and keeping only first order terms, one obtains

$$\frac{\partial z}{\partial t}(\zeta, t) + \frac{\partial z}{\partial \zeta}(\zeta, t) \frac{d\zeta}{dt} = v_r - \frac{\sigma_0 |v_r|}{g(v_r)} z(\zeta, t) \tag{53}$$

Using the fact that $d\zeta/dt = |\omega r|$ we have the following partial differential equation for the internal friction state along the patch

$$\frac{\partial z}{\partial t} + \frac{\partial z}{\partial \zeta} |\omega r| = v_r - \frac{\sigma_0 |v_r|}{g(v_r)} z \tag{54}$$

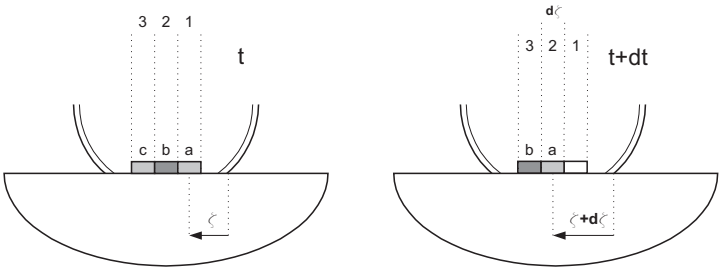

Figure 12: Derivation of distributed friction model along contact patch.

The friction force generated at the patch can be computed from

$$F(t) = \int_0^L dF(\zeta, t) d\zeta \tag{55}$$

The friction force developed in the element $d\zeta$ is given by

$$dF(\zeta,t) = \left(\sigma_0 z(\zeta,t) + \sigma_1 \frac{\partial z}{\partial t}(\zeta,t) + \sigma_2 v_r\right) f_n(\zeta) \tag{56}$$

where $f_n(\zeta)$ is the normal force density function along the patch, and $dF(\zeta,t)$ is the friction force induced by the element at position ζ of the patch, at time t. The total friction force at the patch, can thus be computed as follows

$$F(t) = \int_0^L (\sigma_0 z(\zeta,t) + \sigma_1 \frac{\partial z}{\partial t}(\zeta,t) + \sigma_2 v_r) f_n(\zeta)\, d\zeta \tag{57}$$

Calculations of the decaying force distribution Eq. (33) Assuming (33) we get

$$\begin{aligned}
&\int_0^L \sigma_0 z_{ss}(\zeta) f_n(\zeta)\, d\zeta \\
= \;& \sigma_0 \int_0^L c_2(1-e^{C\zeta}) f_{n0} a^{\frac{\zeta}{L}} d\zeta = \sigma_0 c_2 f_{n0} \int_0^L (1-e^{C\zeta}) a^{\frac{\zeta}{L}} d\zeta \\
= \;& \sigma_0 c_2 f_{n0} \Big[\frac{L}{\ln a} e^{\frac{\ln a}{L}\zeta} - \frac{L}{\ln a + CL} e^{(\frac{\ln a}{L}\zeta + C\zeta)}\Big]_0^L \\
= \;& \sigma_0 c_2 f_{n0} \Big(\frac{L}{\ln a} e^{\ln a} - \frac{L}{\ln a + CL} e^{(\ln a + CL)} - \frac{L}{\ln a} + \frac{L}{\ln a + CL}\Big) = \\
= \;& \sigma_0 c_2 \frac{f_{n0} L}{\ln a} \Big(e^{\ln a} - \frac{\ln a}{\ln a + CL} e^{(\ln a + CL)} - 1 + \frac{\ln a}{\ln a + CL}\Big)
\end{aligned}$$

Similarly,

$$\begin{aligned}
\int_0^L \sigma_2 v_r f_n(\zeta) d\zeta \;&=\; \\
&= \sigma_2 v_r \int_0^L f_n(\zeta) d\zeta = \sigma_2 v_r \int_0^L a^{\frac{\zeta}{L}} f_{n0} d\zeta \\
&= \sigma_2 v_r f_{n0} \Big[\frac{L}{\ln a} a^{\frac{\zeta}{L}}\Big]_0^L = \sigma_2 v_r f_{n0} \Big[\frac{L}{\ln a} a - \frac{L}{\ln a}\Big] \\
&= \sigma_2 v_r \frac{f_{n0} L}{\ln a}(a-1)
\end{aligned}$$

Finally we have,

$$F_{ss} = \sigma_0 c_2 k_1 \Big(e^{\ln a} - k_2 e^{(\ln a + CL)} - 1 + k_2\Big) + \sigma_2 v_r k_1 (a-1) \tag{58}$$

with the constant as defined in the main body of the paper.

Acknowledgements

The first two authors would like to acknowledge support from CNRS and NSF(award no. INT-9726621/INT-9996096), for allowing frequent visit between the School of

Aerospace Engineering at the Georgia Institute of Technology and the Laboratory of Automatic Control of Grenoble. These visit led to the development of the dynamic friction model presented in this paper. The first author would like to thank M. Sorine and P.A. Bliman for interesting discussions on distributed friction models, and to X. Claeys for his remarks on the first version of the model.

References

[1] Bernard, J., and Clover, C. L. (1995), Tire Modeling for Low-Speed and High-Speed Calculations. Society of Automotive Engineers Paper # Paper 950311.

[2] Bakker, E., L. Nyborg, and H. Pacejka, "Tyre Modelling for Use in Vehicle Dynamic Studies," Society of Automotive Engineers Paper # 870421, 1987.

[3] Bliman, P.A., T. Bonald, and M. Sorine, "Hysteresis Operators and Tire Friction Models: Application to vehicle dynamic Simulator," *Prof. of ICIAM. 95*, Hamburg, Germany, 3-7 July, 1995.

[4] Burckhardt, M. (1987). ABS und ASR, Sicherheitsrelevantes, Radschlupf-Regel System, *Lecture Scriptum*. University of Braunschweig, Germany.

[5] Burckhardt, M., *Fahrwerktechnik: Radschlupfregelsysteme*. Vogel-Verlag, Germany, 1993.

[6] Canudas de Wit, C., H. Olsson, K. J. Åström, and P. Lischinsky, "A New Model for Control of Systems with Friction," *IEEE TAC*, Vol. 40, No. 3, pp. 419-425, 1995.

[7] Canudas de Wit, C., R. Horowitz, R. and P. Tsiotras, "Model-Based Observers for Tire/Road Contact Friction Prediction," In *New Directions in Nonlinear Observer Design*, Nijmeijer, H. and T.I Fossen (Eds), Springer Verlag, Lectures Notes in Control and Information Science, May 1999.

[8] Canudas de Wit, and P. Tsiotras, "Dynamic tire friction models for vehicle traction control," In *Proceedings of the IEEE Conference on Decision and Control* Phoenix (Arizona, USA), Dec. 1999.

[9] Clover, C. L. and J. E. Bernard, "Longitudinal Tire Dynamics," *Vehicle System Dynamics*, Vol. 29, pp. 231–259, 1998.

[10] Dahl, P. R., "Solid Friction Damping of Mechanical Vibrations," *AIAA Journal*, Vol. 14, No. 12, pp. 1675-1682, 1976.

[11] Deur, J., "Modeling and Analysis of Longutudinal tire dynamics based on the LuGre Friction Model" In *Proceedings of the IFAC conference on Advance in Automotive Control* 28-30 Mars 2001, Kalsruhe, Allemagne .

[12] Faria, L.O. and Oden, J.T. and Yavari, B.T. and Tworzydlo, W.W. and Bass, J.M. and Becker, E.B "Tire Science and Technology" Vol. 20, no. 1, 1992.

[13] Gim, G. and Nikravesh, P. E. (1990), An Unified Semi-Empirical Tire Model with Higher Accuracy and Less Parametersn *SAE International Congress and Exposition*, Detroit-Michigan, 1999.

[14] Harned, J., L. Johnston, and G. Scharpf, Measurement of Tire Brake Force Characteristics as Related to Wheel Slip (Antilock) Control System Design. *SAE Transactions*, Vol. 78 (Paper # 690214), pp. 909–925. 1969.

[15] Kiencke, U. and Daiss, A. (1994). Estimation of Tyre Friction for Enhaced ABS-Systems. In *Proceedings of the AVEG'94*.

[16] Liu, Y. and J. Sun, "Target Slip Tracking Using Gain-Scheduling for Antilock Braking Systems," In *The American Control Conference*, pp. 1178–82, Seattle, WA, 1995.

[17] Maurice, J.P., M. Berzeri, and H.B. Pacejka, "Pragmatic Tyre Model for Short Wavelength Side Slip Variations", In *Vehicle System Dynamics*,31 (1999), pp. 65-94.

[18] Moore, D. F., "The Friction of Pneumatic Tyres", In *Elsevier Scientific Publishing Company*, Amsterdam-Oxford-New York, 1975.

[19] Pasterkamp, W. R. and H. B. Pacejka, "The Tire as a Sensor to Estimate Friction," *Vehicle Systems Dynamics*, Vol. 29, pp. 409-422, 1997.

[20] Pacejka, H. B. and R. S. Sharp, "Shear Force Developments by Psneumatic tires in Steady-State Conditions: A Review of Modeling Aspects," *Vehicle Systems Dynamics*, Vol. 20, pp. 121-176, 1991.

[21] Ramberg W, Osgood WR, "Description of stress-strrain curves by three parameters," *Tech. Note 902*, National Advisory Committee for Aeronautics, Washinton, 1943.

[22] Sargin, M., "Stress-strain relationship for concrete and the analysis of structural concrete sections.," *SM Study 4*, Solid Mechanics Division, University of Waterloo, Canada, 1971.

[23] Wong J. Y., *Theory of Ground Vehicles*. John Wiley & Sons, Inc., New York, 1993.

[24] van Zanten, A., W. D. Ruf, and A. Lutz, "Measurement and Simulation of Transient Tire Forces," in *International Congress and Exposition*, (Detroit, MI). SAE Technical Paper # 890640, 1989.